Published in final edited form as:

Cancer Lett. 2017 March 01; 388: 149–157. doi:10.1016/j.canlet.2016.11.040.

AG311, a small molecule inhibitor of complex I and hypoxia-induced HIF-1α stabilization

Anja Bastian[a], **Satoshi Matsuzaki**[c], **Kenneth M. Humphries**[c], **Gavin A. Pharaoh**[c], **Arpit Doshi**[d], **Nilesh Zaware**[d], **Aleem Gangjee**[d], and **Michael A. Ihnat**[a,b]

[a]Department of Physiology, University of Oklahoma Health Sciences Center, Oklahoma City, OK 73104, United States

[b]Department of Pharmaceutical Sciences, University of Oklahoma College of Pharmacy, Oklahoma City, OK 73117, United States

[c]Oklahoma Medical Research Foundation, Oklahoma City, OK 73104, United States

[d]Division of Medicinal Chemistry, Graduate School of Pharmaceutical Sciences, Duquesne University, Pittsburgh, PA 15282, United States

Abstract

Cancer cells have a unique metabolic profile and mitochondria have been shown to play an important role in chemoresistance, tumor progression and metastases. This unique profile can be exploited by mitochondrial-targeted anticancer therapies. A small anticancer molecule, AG311, was previously shown to possess anticancer and antimetastatic activity in two cancer mouse models and to induce mitochondrial depolarization. This study defines the molecular effects of AG311 on the mitochondria to elucidate its observed efficacy. AG311 was found to competitively inhibit complex I activity at the ubiquinone-binding site. Complex I as a target for AG311 was further established by measuring oxygen consumption rate in tumor tissue isolated from AG311-treated mice. Cotreatment of cells and animals with AG311 and dichloroacetate, a pyruvate dehydrogenase kinase inhibitor that increases oxidative metabolism, resulted in synergistic cell kill and reduced tumor growth. The inhibition of mitochondrial oxygen consumption by AG311 was found to reduce HIF-1α stabilization by increasing oxygen tension in hypoxic conditions. Taken together, these results suggest that AG311 at least partially mediates its antitumor effect through inhibition of complex I, which could be exploited in its use as an anticancer agent.

Keywords

anticancer compound; mitochondrial metabolism; electron transport chain; hypoxia; NADH-ubiquinone oxidoreductase

Corresponding Author: Michael A. Ihnat, PhD, Department of Pharmaceutical Sciences, OU College of Pharmacy, PO Box 26901, Oklahoma City, OK 73126-0901, Phone: 271-6593 ext. 47965, michael-ihnat@ouhsc.edu.

1. INTRODUCTION

In addition to genetic and epigenetic heterogeneity, the concept of metabolic heterogeneity has increased recently. Considerable heterogeneity exists between different tumors, but also within the same tumor. This intratumoral heterogeneity is predominately mediated by genetic diversity; energy demand; and the proximity to vasculature, dictating glucose and oxygen availability. Until recently, cancer cells were thought to rely only on glycolysis for ATP production, even in the presence of sufficient oxygen supply [1], but metabolic heterogeneity demonstrates that there are multiple metabolic phenotypes, going beyond the upregulated glycolysis as observed by Warburg. One of these metabolic phenotypes is mitochondrial respiration, as cancer cells have been shown to have functional mitochondria capable of producing ATP [2–4].

Anticancer agents acting through mitochondrial inhibition have been described. For example, the anti-diabetic biguanides metformin and phenformin have been shown to exert their anticancer effect by inhibiting complex I, the first enzyme in the mitochondrial electron transport chain (ETC) [5–8]. BAY-87-2243, another complex I inhibitor, has shown efficacy in a preclinical model of resistant melanoma [9]. The small molecule, IACS-10759, was specifically designed as a complex I inhibitor to target chemoresistant dormant tumors [9,10]. Complex I, NADH-ubiquinone oxidoreductase, is a crucial player in mitochondrial respiration. It transfers electrons from NADH to reduce ubiquinone to ubiquinol resulting in proton translocation into the mitochondrial intermembrane space, which establishes an electrochemical gradient that is used for ATP synthesis. In order for this process to continue, molecular oxygen is required as the final electron acceptor. Regions of solid tumors often exhibit low oxygen tension (hypoxia), which has been shown to be involved in tumor development, chemo- and radioresistance, and metastasis in addition to tumor bioenergetics [11,12]. These alterations in bioenergetic processes are mediated in part by increasing gene expression involved in glycolysis and by lowering the activity of the electron transport chain [13–15]. The major cellular adaptive response to hypoxia is tightly regulated by hypoxia-inducible transcription factor-1α, HIF-1α, which is stabilized in low oxygen tensions, thus an inhibition of complex I can prevent electron transfer and decrease oxygen consumption, which in turn could decrease HIF-1α stabilization [16,17]. HIF-1α is capable of inducing a broad range of cellular responses including angiogenesis, resistance to apoptosis and tumor energetics/metabolism. Due to the importance of mitochondrial oxidative phosphorylation in hypoxia and in supporting tumor growth, progression and metastasis [18,19], the development of mitochondrial inhibitors seems well justified.

Herein we investigate the molecular mechanism of a small molecule antitumor agent, AG311. We have previously shown that AG311 significantly reduced primary tumor growth and lung metastases in two breast cancer mouse models, by 81–85% [20]. Upon further investigation, a distinct metabolic mechanism for AG311 emerged. We reported that AG311 rapidly induced necrotic cell death, depolarized the mitochondrial membrane and severely reduced intracellular ATP levels [20]. In the current study, we further define the molecular and antitumor mechanisms and identify complex I of the electron transport chain (ETC) as a likely molecular target of AG311 in isolated cells and in tumors. We show that as a downstream consequence of complex I inhibition, AG311 reduced hypoxia-induced HIF-1α

stabilization. Additionally, we show that AG311 synergizes with dichloroacetate (DCA), which reverses the Warburg effect, in cancer cells and in a xenograft tumor mouse model.

2. MATERIALS & METHODS

Additional information is described in the supplemental methods

2.1. Cell culture—Cancer cell lines were purchased from American Type Culture Collection (Manassas, VA), except MDA-MB-435, which was a kind gift of Dr. Janet Price at MD Anderson Cancer Center in the mid-1990s. MDA-MB-435 are poorly differentiated basal-like breast cancer cells that express melanocytic molecular markers [21–23]. Cell lines were maintained as previously described [20]. Hypoxia culture was performed in 1.5% O_2 with 5% CO_2 using in Invivo$_2$400 (Ruskinn, Leeds, UK).

2.2. Viability assay—Cells were treated with AG311 or for the synergy experiment treated in combination with dichloroacetate (DCA) (SigmaAldrich, St. Louis, MO) at various concentrations. The drugs were diluted in OptiMEM at the final concentration (LifeTechnologies). After 24 or 48 hours, viability was determined with PrestoBlue (Invitrogen, Carlsbad, CA) according to manufacturer's instructions and read with a microplate reader (BioTek, Winooski, VT). Combination index (CI) values were determined using Chou-Talalay method with CompuSyn software [24]. Where noted, total live cell count was determined by labeling nuclei with Hoechst 33342 (2 μg/ml) (LifeTechnologies) and dead cells with the membrane impermeable dye SytoxGreen (0.5 μM) (LifeTechnologies) followed by imaging with Operetta High-Content Imaging System (PerkinElmer, Waltham, MA)

2.3. Cytotoxic compound—The initial design and synthesis of AG311 was conducted by A. Gangjee and N. Zaware [25]. For cell culture experiments, AG311 was prepared as a 50 mM stock and diluted in cell culture medium with a final DMSO concentration not exceeding 0.2%.

2.4. Cellular ATP content measurement—Cells were treated with AG311 in OptiMEM for the indicated durations. The cells were lysed in 20 μL OptiMEM with 20 μL lysis buffer per well and 10 μL of lysate was added to assess ATP levels using ATP Detection Assay Kit (Abcam, Cambridge, MA) according to manufacturer’s instructions. The data were normalized to ATP content of untreated cells.

2.5. Mitochondrial membrane potential—Mixed or monoculture were prepared as previously described [20]. For mixed culture, HMEC-1 and MDA-MB-435 cells were incubated with Cell Tracker Green (1 μM) or Cell Tracker Blue (25 μM) (LifeTechnologies). Cells were incubated with TMRM at 10 nM (Biotium, Hayward, CA) in OptiMEM for 30 min, followed by treatment with AG311 and imaging with Operetta.

2.6. Electron transport chain enzymatic analyses—The enzymatic activity of complex I, III, IV of the electron transport chain was measured spectrophotometrically in the presence of AG311 or solvent as previously described [26].

2.7. MDA-MB-435 orthotopic xenograft—The animal experiments described in this study were approved by the Institutional Animal Care and Use Committee of OUHSC. The detailed methods for this model have been described previously [27]. Five days after tumor implantation, nu/nu mice were treated intraperitoneally twice weekly with AG311 (37 mg/kg) or solvent control (described in supplemental methods). DCA was administered in the drinking water at 50 mg/kg.

2.8. Oxygraphic measurements using Seahorse—Cells (MDA-MB-435) were seeded in Seahorse Flux Analyzer plate (6500 cells/well) coated with Cell-Tak adhesive coating (Corning, Corning, NY) and incubated overnight at 37°C, 5% CO_2 in DMEM. Cell media was replaced with XF Assay Medium containing 25 mM glucose. Seahorse XFe96 analyzer was used to record OCR (oxygen consumption rate) in response to injection of solvent (DMSO) or AG311.

2.9. Oxygraphic measurements using Oroboros—Freshly isolated tumor tissue from untreated or AG311-treated mice was prepared for oxygraphic measurements as previously described [28,29]. Tumors from AG311-treated mice were excised 1 hour after intraperitoneal injection with a 45 mg/kg dose.

2.10. Western Blot—Western blots were incubated with HIF-1α antibody (1:1000, #3716, Cell Signaling, Danvers, MA), p-αAMPK antibody (1:1000, #2535, Cell Signaling), αAMPK antibody (1:1000, #2603, Cell Signaling) overnight at 4°C. Levels of β-actin (Cell Signaling #4970) (1:1000) or vinculin (SigmaAldrich) (1:4000) were used as the loading control. Densitometry was performed using Image Lab software v5.2.1 (Bio-Rad, Hercules, CA). Values are represented as the ratio of target protein to loading control. For the HIF-1α blot using MDA-MB-435 cell lysate, unrelated lanes between the AG311-treated samples and $CoCl_2$ control were removed. The image was spliced together at that position.

2.11. Semi-quantitative real-time polymerase chain reaction (PCR)—Real-time PCR was performed with cDNA as described previously [30]. Quantitative values of target genes for hypoxic conditions were first normalized to 28S rRNA content using the ddCt method [31] and then normalized to the corresponding normoxic control.

2.12. Immunocytochemistry—Immunocytochemistry was performed using isothiocyanate (FITC)-labeled anti-pimonidazole antibody (Hypoxyprobe Inc, Burlington, MA) [32].

3. RESULTS

3.1. Preferential cytotoxicity in glucose-deprived cancer cells and mitochondrial depolarization by AG311

Because cancer cells have an increased energy demand, induction of metabolic stress with glucose-depleted media can sensitize them to mitochondrial inhibitors. AG311 showed enhanced cytotoxicity in cancer cells (MDA-MB-435) treated in glucose-depleted medium, whereas docetaxel did not show a differential effect (Fig 1A). AG311 has been shown to cause rapid mitochondrial membrane depolarization in cancer cells [20]. The mitochondrial

depolarization was more profound in cancerous cells (MDA-MB-435), compared to noncancerous human microvascular endothelial cells (HMEC-1) (Fig 1B). To begin to characterize the functional role of this mitochondrial depolarization, ATP levels were measured. Cells (MDA-MB-435 and HMEC-1) treated with AG311 for four hours showed mitochondrial depolarization which correlated with a decline in intracellular ATP. Cancerous cells were more sensitive to ATP depletion by AG311 compared to noncancerous HMEC-1. (Fig 1C). No effect on viability was observed at this early time point (data not shown). This suggests a potential functional association between AG311-induced mitochondrial disruption and ATP depletion.

3.2. Electron transport chain (ETC) complex I and III inhibition by AG311

To establish a direct effect of AG311 on the mitochondria, ETC activity in the presence of AG311 was examined. Initial enzymatic experiments were performed using solubilized mitochondria isolated from kidney (Fig 2A–D) and confirmed with lysates from MDA-MB-435 and MDA-MB-231 cancer cells (Fig 2E). AG311 most potently inhibited complex I activity (IC_{50}=9.9 μM) compared to complex III-IV (ubiquinol oxidase) activity (IC_{50}=20.2 μM) (Fig 2A). The IC_{50} for complex I inhibition are comparable to the EC_{50} values for cancer cell death (13.9 μM). To determine whether the reduced ubiquinol oxidase activity was due to complex III or IV inhibition, complex IV-specific cytochrome c oxidation activity was measured. AG311 had no effect on complex IV activity, thus the observed complex III-IV inhibition of AG311 can be attributed to a direct effect on complex III (Fig 2A). Further enzyme kinetic studies were performed to determine the type of inhibition of complex I and III by increasing ubiquinone or ubiquinol concentrations, respectively. AG311 competitively inhibited ubiquinone binding to complex I with an inhibitor constant (Ki) of 0.84 μM (Fig 2B). Rotenone (3 nM), a known complex I inhibitor, potently inhibited complex I activity. In contrast to complex I inhibition, the Ki for complex III by AG311 was much higher, Ki=32 μM, and the inhibition was found to be noncompetitive for ubiquinol binding (Fig 2C). Because AG311 inhibits complex I with a much lower Ki as compared to complex III, increased focus was placed on complex I inhibition. For additional evidence that AG311 acts at the ubiquinone-binding site, the NADH:ferricyanide oxidoreductase assay was used. In this assay, the NADH oxidation reaction is localized entirely to the flavin site on complex I and eliminates the need for ubiquinone as an electron acceptor [33]. Therefore, if AG311 competes with ubiquinone for binding, no inhibition should be observed by AG311. Indeed, at various concentrations, AG311 did not inhibit ferricyanide reductase activity (Fig 2D). This effect is similar to rotenone, which also is a competitive inhibitor for the ubiquinone-binding site [34] (Fig 2D). The inhibition of complex I by AG311 was next confirmed using lysates from two cancer cell lines. The IC_{50} values were comparable to the ones obtained using solubilized kidney mitochondria with 11.9 μM for MDA-MB-435 and 6.9 μM for MDA-MB-231 (Fig 2E).

3.3. Combination of DCA and AG311 augments cytotoxicity and anti-tumor effects

Next, it was of interest to determine whether increasing mitochondrial activity with dichloroacetate (DCA) would synergize with AG311-mediated mitochondrial inhibition. DCA functions to increase mitochondrial activity by inhibiting pyruvate dehydrogenase kinase (PDK), a key regulatory enzyme of oxidative metabolism. For this study, MDA-

MB-435 cells were treated with AG311, DCA or both. AG311 alone induced cell death as in previous experiments, while DCA alone had no effect. However, cell viability was significantly reduced by concurrent treatment of DCA with AG311 (Fig 3A). The combination index (CI) was calculated for the dual treatment, with a CI<1 indicating synergy [24]. Three out of the four combinations tested showed synergy with CI values between 0.5 and 0.9, indicating synergistic cytotoxicity (Fig 3A). To test drug synergy *in vivo*, animals bearing orthotopic MDA-MB-435 tumors were treated with either AG311 (37.5 mg/kg IP, twice weekly), DCA (50 mg/kg, daily) or both. The most straightforward synergy experiment is one in which individual treatments have no effect, while the combination produces a significant difference. Thus, for this experiment, the AG311 dose was reduced to 37.5 mg/kg, a dose at which no effect on tumor growth was observed. Previous studies with 45–50 mg/kg AG311 demonstrated significant tumor growth inhibition in two tumor models [20]. The animals treated with both AG311 (37.5 mg/kg twice weekly) and a previously reported innocuous dose of DCA (50 mg/kg/day) [35] showed significantly slower tumor growth compared to solvent or single-drug control animals (Fig 3B). The animal weight was not significantly affected by any of the treatments (Fig 3C).

3.4. AG311 reduces OCR in cells and tumor tissue and increases metabolic stress

To evaluate the effect of complex I inhibition on mitochondrial function, the oxygen consumption rate (OCR) was assessed in response to AG311 *in vitro*-treated cells, in *ex vivo*-treated tumors and *in situ* after systemic treatment. For the cellular studies, the OCR was measured before and after injection of AG311 into wells containing MDA-MB-435 cells in glucose media. AG311 (5 and 10 μM) rapidly and significantly reduced OCR, which correlates with its inhibitory effect on complex I (Fig 4A). For the *ex vivo* studies, tumors from untreated mice were excised. The permeabilized tumor slices were used to measure the effect of AG311 on tumor OCR. The study was carried out with the complex I substrates glutamate and malate (GM). In the presence of AG311 (15 μM), the OCR of tumor slices was significantly reduced (Fig 4B). For the *in situ* tumor studies, the OCR was measured using tumor slices isolated from mice one hour after IP injection with solvent or AG311 (this time with a therapeutic dose of AG311, 45 mg/kg twice weekly). The treatment of animals with AG311 resulted in a significant reduction in tumor OCR in the presence of GM (Fig 4C). The reduced OCR observed here can be attributed to the inhibition of complex I rather than complex II, because AG311 only inhibited OCR in the presence of the NADH-generating substrates GM, but not in the presence of complex II substrate, succinate (Fig 4D). The remaining tumor tissue was used for protein isolation to evaluate phosphorylation of AMP-activated protein kinase (AMPK) which, similar to reduced OCR, is a measurable downstream effect of mitochondrial inhibition. As a result of mitochondrial inhibition, the AMP/ATP ratio increases, which stimulates the phosphorylation of AMPK as a sensor of metabolic stress [36]. AG311-treated tumors showed an overall average increase in p-AMPK levels, although not all samples showed an increase (Fig 4E). This suggests that complex I inhibition leads to reduced ATP production in the tumors similar to the observation in cancer cells (Fig 1C). Together these data indicate that AG311 not only inhibits complex I in cancer cells, but also in tumors.

3.5. AG311 prevents HIF-1α stabilization in hypoxia and increases cellular oxygen content

It has been demonstrated that inhibition of oxygen consumption by complex I inhibitors reduces the stabilization of HIF-1α in hypoxia [7,17]. Since AG311 reduces OCR (Fig 4A–C) and this could increase the cellular oxygen availability, the effect of AG311 on HIF-1α in hypoxic conditions was examined. A narrow range of AG311 doses was tested due to its steep-dose response curve, since a slightly higher dose (20 μM) than those used here results in complete and rapid cell death [20]. AG311 prevented hypoxia-induced accumulation of HIF-1α protein in cancer cells (MDA-MB-435 and MDA-MB-231) (Fig 5A). To examine whether this inhibition was functional, the expression of two HIF-1α-induced target genes was assessed. AG311 significantly reduced the mRNA expression of both vascular endothelial growth factor (pan- VEGF-A) and carbonic anhydrase 9 (CA9) in hypoxic MDA-MB-435 and MDA-MB-231 cells compared to the corresponding normoxic controls (Fig 5B and 5C, respectively). Further, pretreatment with MG-132, a proteasome inhibitor, partially restored HIF-1α levels in the presence of AG311 in MDA-MB-435 cells (Suppl. Fig S1), suggesting that AG311 reduces HIF-1α protein stabilization and promotes its degradation. To determine whether AG311 affects localized cellular hypoxia, cells were preincubated with pimonidazole, a common hypoxia marker which forms adducts under hypoxic conditions [37,38]. Interestingly, treatment of MDA-MB-435 and MDA-MB-231 cells with AG311 attenuated the accumulation of pimonidazole adducts (Fig 5D), indicating that the mitochondrial inhibition by AG311 prevents the decrease of intracellular oxygen tension in response to hypoxia. In summary, under hypoxic conditions, AG311-induced reduction in oxygen consumption results in increased oxygen tension, which in turn reduces HIF-1α stabilization.

4. DISCUSSION

As a continuation of our previous findings showing that AG311 depolarizes mitochondrial membrane potential and induces necrotic cell death, here we explored the effect of AG311 on mitochondria function. We show that the AG311-induced mitochondrial membrane depolarization was more pronounced in cancerous cells as compared to normal cells (Fig 1B). In an endeavor to identify the molecular target of AG311, ETC complexes were tested. It was found that AG311 potently inhibited complex I of the ETC, and to a lesser degree complex III. The observed mitochondrial depolarization and ATP depletion with AG311 are likely a result of this inhibition. Complex I is a large multi-subunit enzyme with multiple potential binding sites. Here, we identified that AG311 inhibits complex I activity by competing with ubiquinone for its binding site on complex I (Fig 2B). It could be expected that the AG311 effect on complex III, similar to complex I, is due to competition with ubiquinol for its binding site on complex III. However, data thus far indicates this inhibition is noncompetitive (Fig 2C), suggesting that AG311 binds to a yet unidentified site on complex III.

We next showed that AG311 synergizes with DCA *in vitro* and in a tumor model to reduce cell viability and tumor volume, respectively (Fig 3A, B). This synergistic effect could be explained by DCA causing reversal of the glycolytic phenotype and increasing reliance on mitochondrial metabolism for cellular energy production [39], thus making cells more

susceptible to mitochondrial complex I inhibition by AG311 [40]. Animals treated with both AG311 and DCA did show reduced weight gain, although this was not significant in this short-term experiment. That said, additional studies with increased AG311 doses will be conducted to further evaluate the therapeutic potential of this combination.

The inhibition of complex I by AG311 slows down electron transfer and reduces the mitochondrial oxygen consumption rate (OCR). This was not only observed in cancer cells (Fig 4A), but also in tumor tissue from AG311-treated animals (Fig 4C). These results demonstrate that AG311 accumulates at a sufficient concentration in tumor tissue to reduce complex I activity. Reduced complex I activity results in energy stress as characterized by the increase in AMP/ATP ratio and subsequent activation of AMPK, as shown in tumors from AG311-treated mice (Fig 4E). Although this data supports the idea that AG311 inhibits complex I, the activation of AMPK by AG311 also raises the potential for resistance due to AMPK-mediated survival [41,42]. This activation of AMPK requires the upstream kinase LKB1, which has been characterized as a tumor suppressor [43]. LKB1-mediated activation of AMPK could make cells more resistant as the cells would be able to cope with energetic stress imposed by mitochondrial inhibitors [44]. It has been demonstrated that some human cancers, such as non-small cell lung carcinoma (NSCLC), are frequently deficient in LKB1, rendering them more sensitive to energetic stress induced by mitochondrial inhibitors [45]. Thus, AG311 may be particularly efficacious in LKB1-deficient tumors, as has been shown with metformin [46].

Reducing mitochondrial OCR by AG311 could prove therapeutically beneficial by preventing the induction of a HIF-1α-mediated cytoprotective response to hypoxia. We demonstrate that decreased OCR in response to AG311 is accompanied by increased cellular oxygen tension and by HIF-1α degradation in hypoxic conditions (Fig 5). Our data suggests that the observed HIF-1α degradation during hypoxia is likely due to a localized increase in oxygen tension mediated by AG311. However, an alternative explanation is that AG311 inhibition of complex I could result in an accumulation of the TCA metabolite, α-ketoglutarate, which in turn activates HIF-1α prolyl hydroxylating enzymes, PHDs, leading to HIF-1α degradation [47,48]. This HIF-1α degradation could explain, in part, the previously reported anti-angiogenic effect of AG311 [25]. This HIF-1α destabilization by AG311 could also play a role in overcoming radioresistance [11], by re-oxygenating hypoxic tumor regions and sensitizing them to radiation therapy [49,50]. More recently, HIF-1α has been shown to induce the expression of the immune checkpoint inhibitor PD-L1 in response to hypoxia, preventing tumor attack by cytotoxic T-cells [51,52]. In future studies, it would be interesting to investigate the effect of AG311 on PD-L1 expression.

AG311 combines multiple anticancer mechanisms (inhibition of tyrosine kinases, thymidylate synthase, and complex I) and has been demonstrated to have antitumor and anti-metastatic effects in vivo [20]. The anti-metastatic effect could be explained in part by the effect of AG311 on the mitochondrial respiration. Mitochondria have been shown to be necessary for metastatic progression [19]; and mitochondrial mass is higher in tumor-initiating cells [53]. Nutrient-starved cells grown in tumor spheroids to mimic the dormant/quiescent tumor cells characteristic of metastases have been shown to be more sensitive to mitochondrial inhibitors [54–56]. In keeping with this idea, cells under glucose-limiting

conditions have been shown to upregulate nuclear encoded OXPHOS genes for ATP production [57]. To elucidate the specific contribution of complex I inhibition to AG311's anti-metastatic activity will require further investigation.

The biguanides metformin and phenformin have attracted the most attention as potential anticancer complex I inhibitors as they were already FDA approved (for diabetes) and metformin has a relatively mild adverse effect profile [6,7,45,57]. However, metformin and its more potent analog, phenformin, have high IC_{50} values for complex I inhibition: 20 mM, 0.5 mM, respectively [6]. Metformin (but not phenformin) relies on the expression of an organic cation transporter, OCT, for its absorption [58]. In contrast to the biguanides, BAY-87-2243, a new complex I inhibitor, has nanomolar potency, but its major limitation is its specificity for *human* complex I, limiting its preclinical evaluation using other species [59]. A series of marine toxins including mycothiazole, furospongolide, lehualide B, and kalkitoxin have recently been identified as complex I inhibitors and disruptors of HIF-1α signaling in hypoxic cancer cells [60]. Limitations of these toxins, as the moniker implies, are potential toxic off-target effects such as N-methyl-D-aspartate (NMDA)-mediated neurotoxicity by kalkitoxin [60]. In comparison to these complex I inhibitors, the IC_{50} of AG311 for cancerous cells is in the lower micromolar range and thus falls between the concentrations for biguanides (mM) and BAY-87-2243/toxins (nM). The demonstrated efficacy of AG311 in both human xenograft and mouse allograft studies provides evidence of its inhibition of both mouse and human complex I activity, although this was not directly tested in this work.

Interestingly, evidence exists that RTK (receptor tyrosine kinase) inhibitors such as sorafenib are able to inhibit ETC complexes, although in these reports this effect was more linked to an adverse drug reaction [61,62]. That said, it is possible that complex I inhibition could also contribute to the therapeutic efficacy of these agents. Thus, AG311 inhibition of complex I could link with its previously published RTK inhibitory properties (EGFR, VEGFR, PDGFR), [25] and studies are underway to investigate this relationship.

A potential limitation for the clinical use of AG311 is its steep dose response curve (hillslope=6.8 in isolated cells), indicating that a small change in dosage can result in a large change in cytotoxicity [20], and offering a narrow therapeutic window. To broaden this window and to increase tumor drug delivery, AG311 could be incorporated into nanoparticles. Further, mitochondrial uptake of AG311 could be increased by tethering it to TPP as has been demonstrated with metformin [63]. Although we have shown that AG311 does not induce gross toxicity in this work and in previous publications [20,25], some off-target inhibition would be expected based on a reversible animal lethargy observed shortly after AG311 administration at higher doses.

From a clinical perspective, AG311 could provide an advantage by targeting metabolic tumor heterogeneity and reprogramming. Future experiments using patient-derived xenografts, established and propagated to retain primary tumor heterogeneity, could be used to begin to delineate AG311's potential for targeting heterogeneous tumors [64]. AG311 might also be used clinically as an adjuvant agent with antiproliferative or antiglycolytic

agents, with the latter potentially addressing both metabolic cancer cell phenotypes (oxidative and glycolytic).

Supplementary Material

Refer to Web version on PubMed Central for supplementary material.

Acknowledgments

This work was supported, in part, by the National Institutes of Health, National Cancer Institute [Grant CA136944 (A.G.)], by College of Pharmacy startup funds (M.A.I.), and by a Grant-In-Aid of Research, Sigma Xi (A.B.). The authors acknowledge support from the Presbyterian Health Foundation Equipment grant (College of Pharmacy) and the Institutional Development Award (IDeA) from the National Institutes of Health National Institute of General Medical Sciences [Grant P20-GM103639] (Stephenson Cancer Center Core). The authors also acknowledge support from the Integrative Redox Biology Core in the Oklahoma Nathan Shock Center for Excellence in the Biology of Aging funded by the National Institute on Aging [Grant AG050911].

Abbreviations

NADH	nicotinamide adenine dinucleotide
RTK	receptor tyrosine kinase
TS	thymidylate synthase
CCS	cosmic calf serum
DMSO	dimethyl sulfoxide
HMEC	human microvascular endothelial cells
TMRM	tetramethylrhodamine methyl ester
AMPK	AMP-activated protein kinase
DCA	dichloroacetate
OCR	oxygen consumption rate
OXPHOS	oxidative phosphorylation
α-KG	α-ketoglutarate
TCA	tricarboxylic acid
ETC	electron transport chain
HIF-1α	hypoxia-inducible factor 1-alpha
VEGF	vascular endothelial growth factor
CA9	carbonic anhydrase 9
TKI	tyrosine kinase inhibitor
PHD	prolyl hydroxylase domain

EGFR	epidermal growth factor receptor
PDGFR	platelet-derived growth factor receptors
VEGFR	vascular endothelial growth factor receptor
OCT1	organic cation transporter 1
PD-L1	programmed death-ligand 1

References

1. Gatenby RA, Gillies RJ. Why do cancers have high aerobic glycolysis? Nat Rev Cancer. 2004; 4:891–899. [PubMed: 15516961]
2. Viale A, Corti D, Draetta GF. Tumors and Mitochondrial Respiration: A Neglected Connection. Cancer Res. 2015; 75:3687–3691.
3. Koppenol WH, Bounds PL, Dang CV. Otto Warburg's contributions to current concepts of cancer metabolism. Nat Rev Cancer. 2011; 11:325–337. [PubMed: 21508971]
4. Moreno-Sánchez R, Rodríguez-Enríquez S, Saavedra E, Marín-Hernández A, Gallardo-Pérez JC. The bioenergetics of cancer: Is glycolysis the main ATP supplier in all tumor cells? BioFactors. 2009; 35:209–225. [PubMed: 19449450]
5. Owen MR, Doran E, Halestrap AP. Evidence that metformin exerts its anti-diabetic effects through inhibition of complex 1 of the mitochondrial respiratory chain. Biochem. J. 2000; 348:607–614. [PubMed: 10839993]
6. Bridges HR, Jones AJY, Pollak MN, Hirst J. Effects of metformin and other biguanides on oxidative phosphorylation in mitochondria. Biochem. J. 2014; 462:475–487. [PubMed: 25017630]
7. Wheaton WW, Weinberg SE, Hamanaka RB, Soberanes S, Sullivan LB, Anso E, et al. Metformin inhibits mitochondrial complex I of cancer cells to reduce tumorigenesis. eLife. 2014; 3:e02242. [PubMed: 24843020]
8. Matsuzaki S, Humphries KM. Selective Inhibition of Deactivated Mitochondrial Complex I by Biguanides. Biochemistry. 2015; 54:2011–2021. [PubMed: 25719498]
9. Schöckel L, Glasauer A, Basit F, Bitschar K, Truong H, Erdmann G, et al. Targeting mitochondrial complex I using BAY 87-2243 reduces melanoma tumor growth. Cancer Metab. 2015; 3:11. [PubMed: 26500770]
10. Protopopova M, Bandi M, Bardenhagen J, Bristow C, Carroll C, Chang E, et al. Abstract 4380: IACS-10759: A novel OXPHOS inhibitor which selectively kill tumors with metabolic vulnerabilities. Cancer Res. 2015; 75:4380–4380.
11. Muz B, de la Puente P, Azab F, Azab AK. The role of hypoxia in cancer progression, angiogenesis, metastasis, and resistance to therapy. Hypoxia. 2015:83–92. [PubMed: 27774485]
12. Diers AR, Vayalil PK, Oliva CR, Griguer CE, Darley-Usmar V, Hurst DR, et al. Mitochondrial bioenergetics of metastatic breast cancer cells in response to dynamic changes in oxygen tension: effects of HIF-1α. PLoS ONE. 2013; 8:e68348. [PubMed: 23840849]
13. Wheaton WW, Chandel NS. Hypoxia. 2. Hypoxia regulates cellular metabolism. Am J Physiol Cell Physiol. 2011; 300:C385–C393. [PubMed: 21123733]
14. Tello D, Balsa E, Acosta-Iborra B, Fuertes-Yebra E, Elorza A, Ordóñez Á, et al. Induction of the mitochondrial NDUFA4L2 protein by HIF-1α decreases oxygen consumption by inhibiting Complex I activity. Cell Metab. 2011; 14:768–779. [PubMed: 22100406]
15. Zeng W, Liu P, Pan W, Singh SR, Wei Y. Hypoxia and hypoxia inducible factors in tumor metabolism. Cancer Lett. 2015; 356:263–267. [PubMed: 24508030]
16. Agani FH, Pichiule P, Carlos Chavez J, LaManna JC. Inhibitors of mitochondrial complex I attenuate the accumulation of hypoxia-inducible factor-1 during hypoxia in Hep3B cells. Comp Biochem Physiol a Mol Integr Physiol. 2002; 132:107–109. [PubMed: 12062197]

17. Ellinghaus P, Heisler I, Unterschemmann K, Haerter M, Beck H, Greschat S, et al. BAY 87-2243, a highly potent and selective inhibitor of hypoxia-induced gene activation has antitumor activities by inhibition of mitochondrial complex I. Cancer Med. 2013; 2:611–624. [PubMed: 24403227]
18. Viale A, Corti D, Draetta GF. Tumors and Mitochondrial Respiration: A Neglected Connection. Cancer Res. 2015; 75:3687–3691.
19. Tan AS, Baty JW, Dong L-F, Bezawork-Geleta A, Endaya B, Goodwin J, et al. Mitochondrial genome acquisition restores respiratory function and tumorigenic potential of cancer cells without mitochondrial DNA. Cell Metab. 2015; 21:81–94. [PubMed: 25565207]
20. Bastian A, Thorpe JE, Disch BC, Bailey-Downs LC, Gangjee A, Devambatla RKV, et al. A Small Molecule with Anticancer and Antimetastatic Activities Induces Rapid Mitochondrial-Associated Necrosis in Breast Cancer. J Pharmacol Exp Ther. 2015; 353:392–404. [PubMed: 25720766]
21. Nerlich A. Density-dependent lineage instability of MDA-MB-435 breast cancer cells. Oncol Lett. 2013:1–5.
22. Zhang Q, Fan H, Shen J, Hoffman RM, Xing HR. Human Breast Cancer Cell Lines Co-Express Neuronal, Epithelial, and Melanocytic Differentiation Markers In Vitro and In Vivo. PLoS ONE. 2010; 5:e9712–e9716. [PubMed: 20300523]
23. Sellappan S. Lineage Infidelity of MDA-MB-435 Cells: Expression of Melanocyte Proteins in a Breast Cancer Cell Line. Cancer Res. 2004; 64:3479–3485. [PubMed: 15150101]
24. Chou T-C. Drug combination studies and their synergy quantification using the Chou-Talalay method. Cancer Res. 2010; 70:440–446. [PubMed: 20068163]
25. Gangjee A, Zaware N, Raghavan S, Ihnat M, Shenoy S, Kisliuk RL. Single agents with designed combination chemotherapy potential: synthesis and evaluation of substituted pyrimido[4,5-b]indoles as receptor tyrosine kinase and thymidylate synthase inhibitors and as antitumor agents. J. Med. Chem. 2010; 53:1563–1578. [PubMed: 20092323]
26. Matsuzaki S, Szweda LI, Humphries KM. Mitochondrial superoxide production and respiratory activity: biphasic response to ischemic duration. Arch. Biochem. Biophys. 2009; 484:87–93. [PubMed: 19467633]
27. Ihnat MA, Nervi AM, Anthony SP, Kaltreider RC, Warren AJ, Pesce CA, et al. Effects of mitomycin C and carboplatin pretreatment on multidrug resistance-associated P-glycoprotein expression and on subsequent suppression of tumor growth by doxorubicin and paclitaxel in human metastatic breast cancer xenografted nude mice. Oncol. Res. 1999; 11:303–310. [PubMed: 10757444]
28. Kaambre T, Chekulayev V, Shevchuk I, Karu-Varikmaa M, Timohhina N, Tepp K, et al. Metabolic control analysis of cellular respiration in situ in intraoperational samples of human breast cancer. J Bioenerg Biomembr. 2012; 44:539–558. [PubMed: 22836527]
29. Kuznetsov AV, Veksler V, Gellerich FN, Saks V, Margreiter R, Kunz WS. Analysis of mitochondrial function in situ in permeabilized muscle fibers, tissues and cells. Nat Protoc. 2008; 3:965–976. [PubMed: 18536644]
30. Luckett-Chastain LR, Ihnat MA, Mickle-Kawar BM, Gallucci RM. SOCS3 Modulates Interleukin-6R Signaling Preference in Dermal Fibroblasts. J Interferon Cytokine Res. 2012; 32:207–215. [PubMed: 22313262]
31. Livak KJ, Schmittgen TD. Analysis of Relative Gene Expression Data Using Real-Time Quantitative PCR and the 2−ΔΔCT Method. Methods. 2001; 25:402–408. [PubMed: 11846609]
32. Sato Y, Endo H, Okuyama H, Takeda T, Iwahashi H, Imagawa A, et al. Cellular hypoxia of pancreatic beta-cells due to high levels of oxygen consumption for insulin secretion in vitro. J. Biol. Chem. 2011; 286:12524–12532. [PubMed: 21296882]
33. Birrell JA, Yakovlev G, Hirst J. Reactions of the flavin mononucleotide in complex I: a combined mechanism describes NADH oxidation coupled to the reduction of APAD+, ferricyanide, or molecular oxygen. Biochemistry. 2009; 48:12005–12013. [PubMed: 19899808]
34. Prieur I, Lunardi J, Dupuis A. Evidence for a quinone binding site close to the interface between NUOD and NUOB subunits of Complex I. Biochim. Biophys. Acta. 2001; 1504:173–178. [PubMed: 11245783]
35. Ishiguro T. Cotreatment with dichloroacetate and omeprazole exhibits a synergistic antiproliferative effect on malignant tumors. Oncol Lett. 2012

36. Foretz M, Guigas B, Bertrand L, Pollak M, Viollet B. Metformin: from mechanisms of action to therapies. Cell Metab. 2014; 20:953–966. [PubMed: 25456737]
37. Urtasun RC, Koch CJ, Franko AJ, Raleigh JA, Chapman JD. A novel technique for measuring human tissue pO2 at the cellular level. Br J Cancer. 1986; 54:453–457. [PubMed: 3756081]
38. Doege K. Inhibition of mitochondrial respiration elevates oxygen concentration but leaves regulation of hypoxia-inducible factor (HIF) intact. Blood. 2005; 106:2311–2317. [PubMed: 15947089]
39. Sun RC, Fadia M, Dahlstrom JE, Parish CR, Board PG, Blackburn AC. Reversal of the glycolytic phenotype by dichloroacetate inhibits metastatic breast cancer cell growth in vitro and in vivo. Breast Cancer Res Treat. 2009; 120:253–260. [PubMed: 19543830]
40. Choi YW, Lim IK. Sensitization of metformin-cytotoxicity by dichloroacetate via reprogramming glucose metabolism in cancer cells. Cancer Lett. 2014; 346:300–308. [PubMed: 24480191]
41. Wang Z, Liu P, Chen Q, Deng S, Liu X, Situ H, et al. Targeting AMPK Signaling Pathway to Overcome Drug Resistance for Cancer Therapy. Curr Drug Targets. 2016; 17:853–864. [PubMed: 25777274]
42. Jeon S-M, Chandel NS, Hay N. AMPK regulates NADPH homeostasis to promote tumour cell survival during energy stress. Nature. 2012; 485:661–665. [PubMed: 22660331]
43. Zhao RX, Xu ZX. Targeting the LKB1 tumor suppressor. Curr Drug Targets. 2014
44. Chaube B, Bhat MK. AMPK, a key regulator of metabolic/energy homeostasis and mitochondrial biogenesis in cancer cells. Cell Death Dis. 2016; 7:e2044. [PubMed: 26775698]
45. Shackelford DB, Abt E, Gerken L, Vasquez DS, Seki A, Leblanc M, et al. LKB1 Inactivation Dictates Therapeutic Response of Non-Small Cell Lung Cancer to the Metabolism Drug Phenformin. Cancer Cell. 2013; 23:143–158. [PubMed: 23352126]
46. Algire C, Amrein L, Bazile M, David S, Zakikhani M, Pollak M. Diet and tumor LKB1 expression interact to determine sensitivity to anti-neoplastic effects of metformin in vivo. Oncogene. 2010; 30:1174–1182. [PubMed: 21102522]
47. Bunik VI, Buneeva OA, Gomazkova VS. Change in α-ketoglutarate dehydrogenase cooperative properties due to dihydrolipoate and NADH. FEBS Letters. 1990
48. Vatrinet R, Iommarini L, Kurelac I, De Luise M, Gasparre G, Porcelli AM. Targeting respiratory complex I to prevent the Warburg effect. Int. J. Biochem. Cell Biol. 2015; 63:41–45. [PubMed: 25668477]
49. Suzuki Y, Nakano T, Ohno T, Kato S. Oxygenated and reoxygenated tumors show better local control in radiation therapy for cervical cancer. Int J Gynecol Cancer. 2006
50. Helbig L, Koi L, Brüchner K, Gurtner K, Hess-Stumpp H, Unterschemmann K, et al. BAY 87–2243, a novel inhibitor of hypoxia-induced gene activation, improves local tumor control after fractionated irradiation in a schedule-dependent manner in head and neck human xenografts. Radiat Oncol. 2014; 9:207–210. [PubMed: 25234922]
51. Barsoum IB, Smallwood CA, Siemens DR, Graham CH. A mechanism of hypoxia-mediated escape from adaptive immunity in cancer cells. Cancer Res. 2014; 74:665–674. [PubMed: 24336068]
52. Noman MZ, Desantis G, Janji B, Hasmim M, Karray S, Dessen P, et al. PD-L1 is a novel direct target of HIF-1α, and its blockade under hypoxia enhanced MDSC-mediated T cell activation. J. Exp. Med. 2014; 211:781–790. [PubMed: 24778419]
53. Farnie G, Sotgia F, Lisanti MP. High mitochondrial mass identifies a sub-population of stem-like cancer cells that are chemo-resistant. Oncotarget. 2015
54. Senkowski W, Zhang X, Olofsson MH, Isacson R, Hoglund U, Gustafsson M, et al. Three-dimensional cell culture-based screening identifies the anthelmintic drug nitazoxanide as a candidate for treatment of colorectal cancer. Mol. Cancer Ther. 2015; 14:1504–1516. [PubMed: 25911689]
55. Palorini R, Simonetto T, Cirulli C, Chiaradonna F. Mitochondrial complex I inhibitors and forced oxidative phosphorylation synergize in inducing cancer cell death. Int. J. Biochem. Cell Biol. 2013; 2013:1–14.

56. Zhang X, De Milito A, Olofsson M, Gullbo J, D'Arcy P, Linder S. Targeting mitochondrial function to treat quiescent tumor cells in solid tumors. Int. J. Mol. Sci. 2015; 16:27313–27326. [PubMed: 26580606]
57. Birsoy K, Possemato R, Lorbeer FK, Bayraktar EC, Thiru P, Yucel B, et al. Metabolic determinants of cancer cell sensitivity to glucose limitation and biguanides. Nature. 2014; 508:108–112. [PubMed: 24670634]
58. Segal ED, Yasmeen A, Beauchamp M-C, Rosenblatt J, Pollak M, Gotlieb WH. Relevance of the OCT1 transporter to the antineoplastic effect of biguanides. Biochem. Biophys. Res. Commun. 2011; 414:694–699. [PubMed: 21986525]
59. Christian S, Algire C, Schwede W, Mowat JS. Comparison of human-specific versus cross-reactive Complex I inhibitor for in vivo tumor efficacy. Cancer Res. 2016; 76:223–223.
60. Morgan J, Liu Y, Coothankandaswamy V, Mahdi F, Jekabsons M, Gerwick W, et al. Kalkitoxin Inhibits Angiogenesis, Disrupts Cellular Hypoxic Signaling, and Blocks Mitochondrial Electron Transport in Tumor Cells. Marine Drugs. 2015; 13:1552–1568. [PubMed: 25803180]
61. Will Y, Dykens JA, Nadanaciva S, Hirakawa B, Jamieson J, Marroquin LD, et al. Effect of the Multitargeted Tyrosine Kinase Inhibitors Imatinib, Dasatinib, Sunitinib, and Sorafenib on Mitochondrial Function in Isolated Rat Heart Mitochondria and H9c2 Cells. Toxicol. Sci. 2008; 106:153–161. [PubMed: 18664550]
62. Bull VH, Rajalingam K, Thiede B. Sorafenib-Induced Mitochondrial Complex I Inactivation and Cell Death in Human Neuroblastoma Cells. J. Proteome Res. 2012; 11:1609–1620. [PubMed: 22268697]
63. Cheng G, Zielonka J, Ouari O, Lopez M, McAllister DM. Mitochondria-targeted analogs of metformin exhibit enhanced antiproliferative and radiosensitizing effects in pancreatic cancer cells. Cancer Res. 2016
64. Cassidy JW, Caldas C, Bruna A. Maintaining Tumor Heterogeneity in Patient-Derived Tumor Xenografts. Cancer Res. 2015; 75:2963–2968. [PubMed: 26180079]

Highlights

- AG311 competitively inhibits ubiquinone-binding to complex I and prevents electron transfer and mitochondrial respiration.
- Cellular response to hypoxia is reduced by AG311, including HIF-1α protein levels, VEGF, CA9 target genes, and low oxygen tension.
- Combination of AG311 and dichloroacetate augments cytotoxicity and tumor growth reduction.

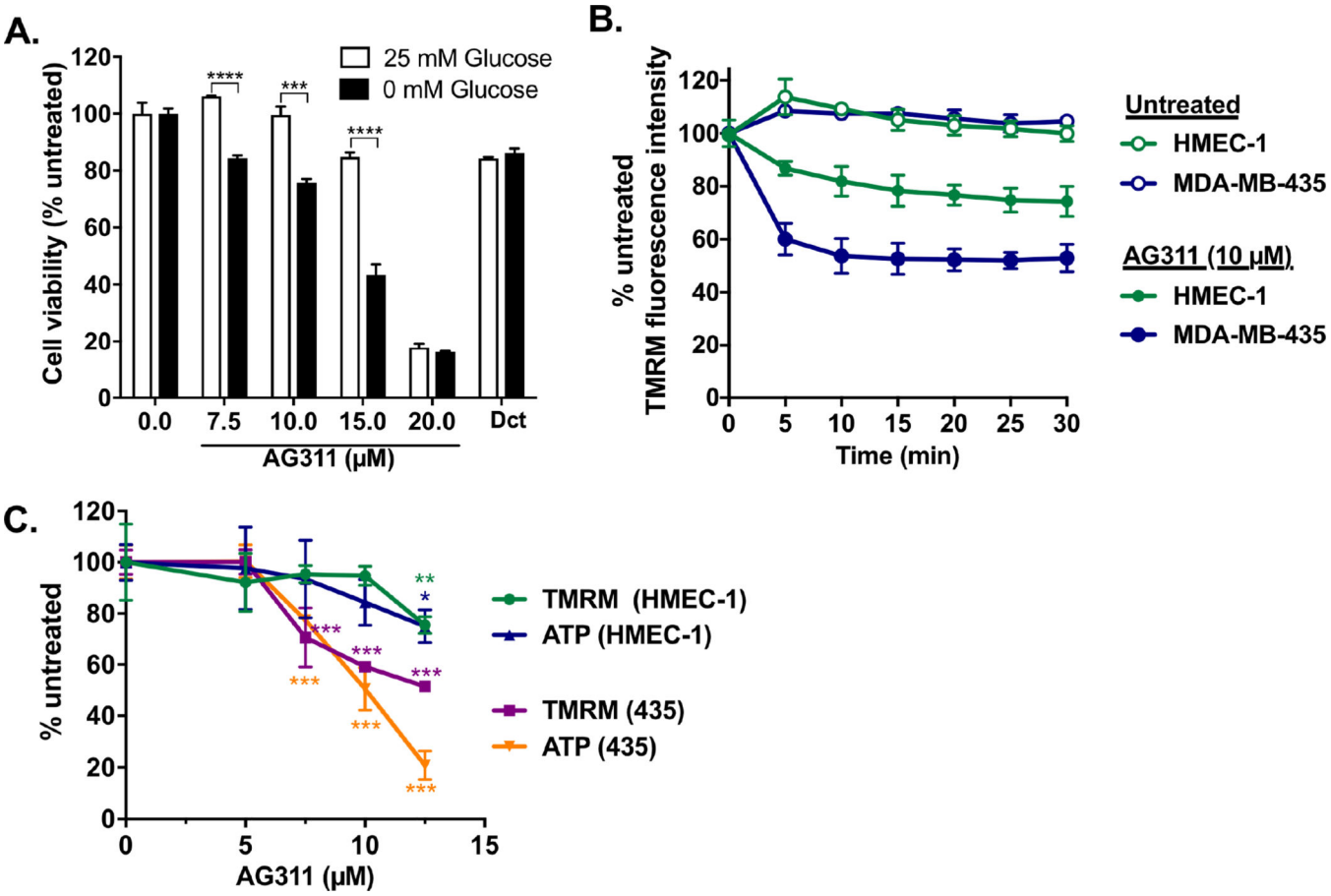

Figure 1. AG311 preferentially reduces viability in glucose-deprived cancer cells and mitochondrial membrane potential in cancer cells

(A) Cell viability of MDA-MB-435 cells treated with AG311 or solvent in media with or without glucose (25 mM) supplementation for 24 hours after 4 hours preincubation in the corresponding media. Docetaxel (Dct) was used as control (1 μM). Viability was assessed with PrestoBlue. **(B)** TMRM fluorescence intensity in response to AG311 was measured every 5 min in MDA-MB-435 cells and HMEC-1, human microvascular endothelial cells. **(C)** MDA-MB-435 cells and HMEC-1 were treated with AG311 or solvent control for 4 hours and then incubated with TMRM and imaged at 10× for fluorescence intensity quantification. ATP levels were measured with a luciferase-based ATP determination kit. n=4 – 6. ***$P \leq 0.05$, ***$P \leq 0.001$, ****$P \leq 0.0001$ versus solvent control.

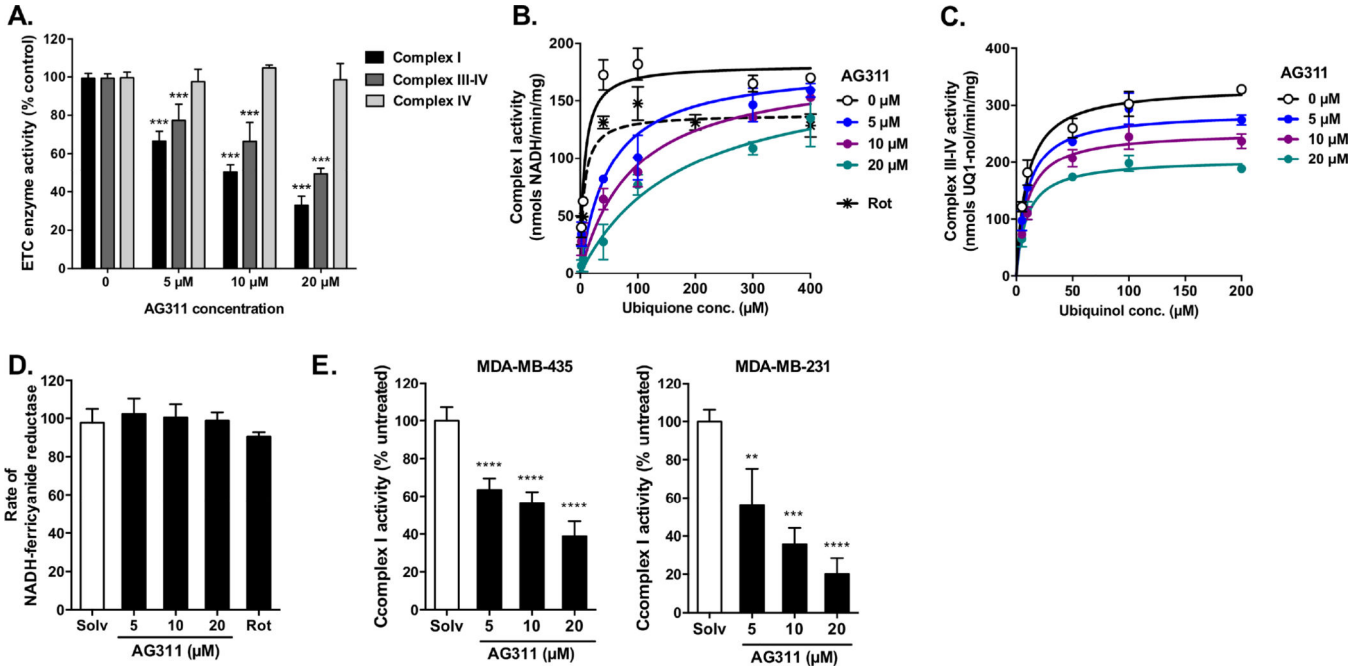

Figure 2. Effect of AG311 on electron transport chain complexes

(A) Effects of AG311 on electron transport chain complex activities were measured spectrophotometrically with solubilized mitochondria isolated from kidney (25 μg/ml). Complex I activity was measured as the oxidation rate of NADH (200 μM) in the presence of antimycin A (50 nM) and ubiquinone (100 μM). Complex III-IV activity was measured as the oxidation rate of ubiquinol (100 μM). Complex IV activity was measured as the oxidation rate of reduced cytochrome c (25 μM), n=6. **(B)** Complex I competition assay for AG311 and ubiquinone was performed with increasing ubiquinone concentrations in the presence AG311 and compared to the uninhibited complex I activity. Rotenone (Rot, 3nM) was used as positive control. **(C)** Complex III-IV competition assay for AG311 and ubiquinol was performed with increasing ubiquinol concentrations in the presence of AG311 and compared to the uninhibited complex III activity. Curves were fitted with GraphPad Prism for competitive and noncompetitive enzyme inhibition. **(D)** Rate of NADH:ferricyanide reductase reaction was measured after addition of solvent, AG311 or rotenone (Rot, 0.1 μM) in the presence of ferricyanide (500 μM) and NADH (200 μM) using solubilized mitochondria isolated from kidney. **(E)** Complex I activity was measured using whole cell lysate (40 μg/ml) from MDA-MB-435 and MDA-MB-231 with or without AG311. (n = 3 – 6). $^{**}P \leq 0.01$, $^{***}P \leq 0.001$, $^{****}P \leq 0.0001$ versus solvent.

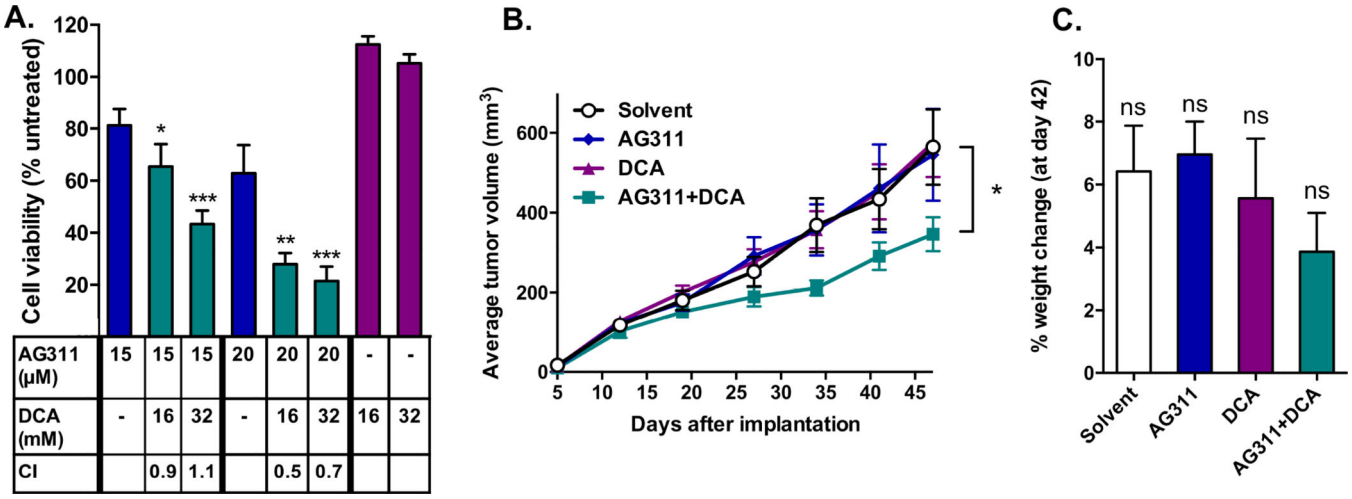

Figure 3. Dichloroacetate (DCA) augments AG311-induced cytotoxicity and tumor growth reduction

(A) Cotreatment with DCA sensitizes MDA-MB-435 cells to AG311. Cell viability was assessed after 24 hours of treatment using PrestoBlue. (n = 4) **(B)** MDA-MB-435 GFP tumor growth curve in an orthotopic xenograft mouse model. Tumor bearing mice (nu/nu) were treated with either solvent control, AG311 (37.5 mg/kg, twice weekly), DCA (50 mg/kg, daily) or with both AG311 and DCA. The dose for AG311 (37.5 mg/kg) was reduced to a non-efficacious level in order to evaluate synergy with DCA. A 45 mg/kg treatment-dose of AG311 alone was previously shown to significantly reduce tumor growth in this model [20]. For statistical analysis, two-way ANOVA repeated measures post-test was used. (n = 9) **(C)** Mouse body weights are shown as percentage change at day 45 over initial weight. (n = 9). $*P \leq 0.05$, $**P \leq 0.01$, $***P \leq 0.001$ versus AG311 alone versus solvent control.

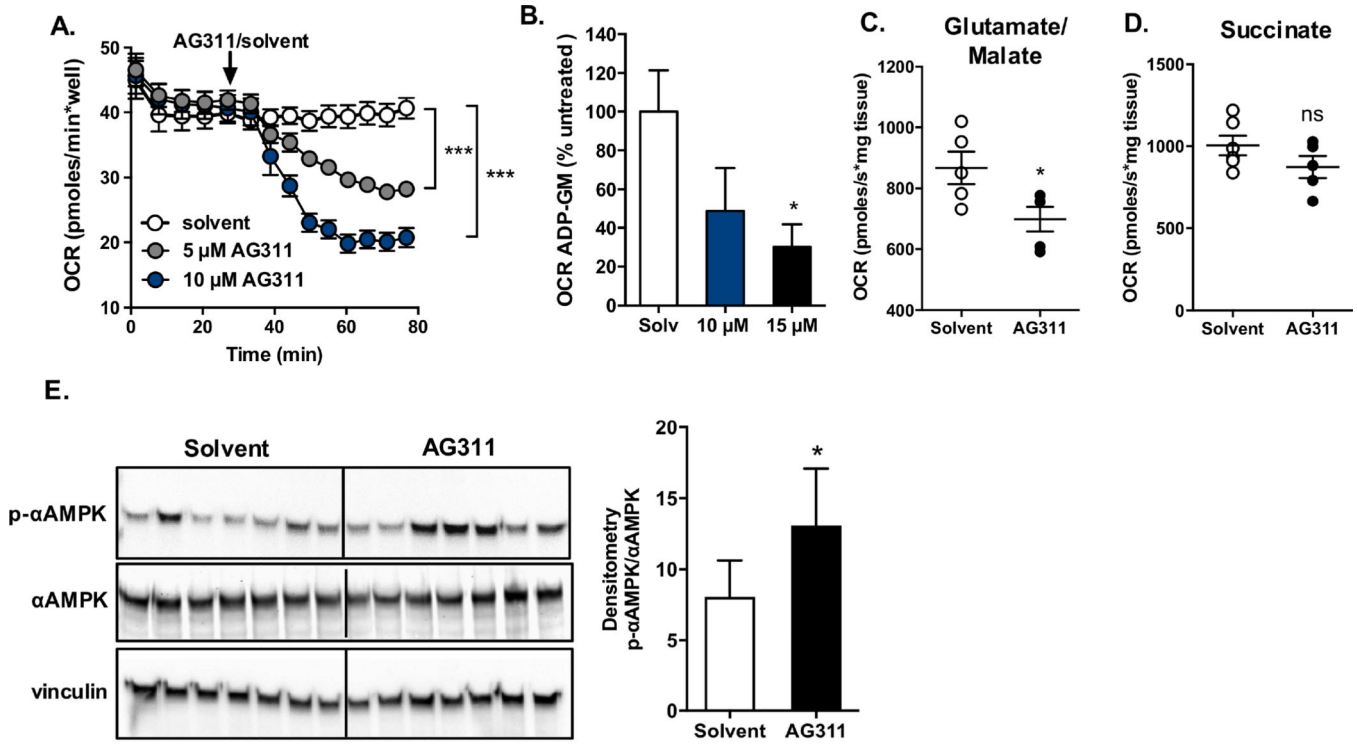

Figure 4. AG311 decreases oxygen consumption rate and increases p-AMPK protein levels

(A). Oxygen consumption rate (OCR) of MDA-MB-231 cells was measured with Seahorse XF^{e}96 Analyzer. **(B, C)** OCR was assessed with Oroboros Oxygraph-2K. (**B**) MDA-MB-435 tumors from mice (nu/nu) were excised, and the permeabilized tissue was treated with AG311 in the presence of glutamate/malate (GM) and ADP to determine the rate of complex I-dependent oxygen consumption. The rate is shown as % untreated of the rate in the presence of GM (background) subtracted from ADP (activated). (n = 3 – 5) (**C**) Tumor bearing mice were treated with AG311 (45 mg/kg) or solvent control and tumor tissue excised for OCR assessment. Data are shown for OCR after addition of glutamate/malate and ADP, (n = 5 – 6). (D) Data are shown for OCR after addition of succinate and ADP, (n = 5 – 6). Data were corrected for residual oxygen consumption using antimycin A. (**E**) Western blot analysis for tumor tissue from AG311- or solvent-treated mice, left panel. Quantification of p-AMPK normalized to total AMPK, right panel. *$P \leq 0.05$, ***$P \leq 0.001$ versus solvent control.

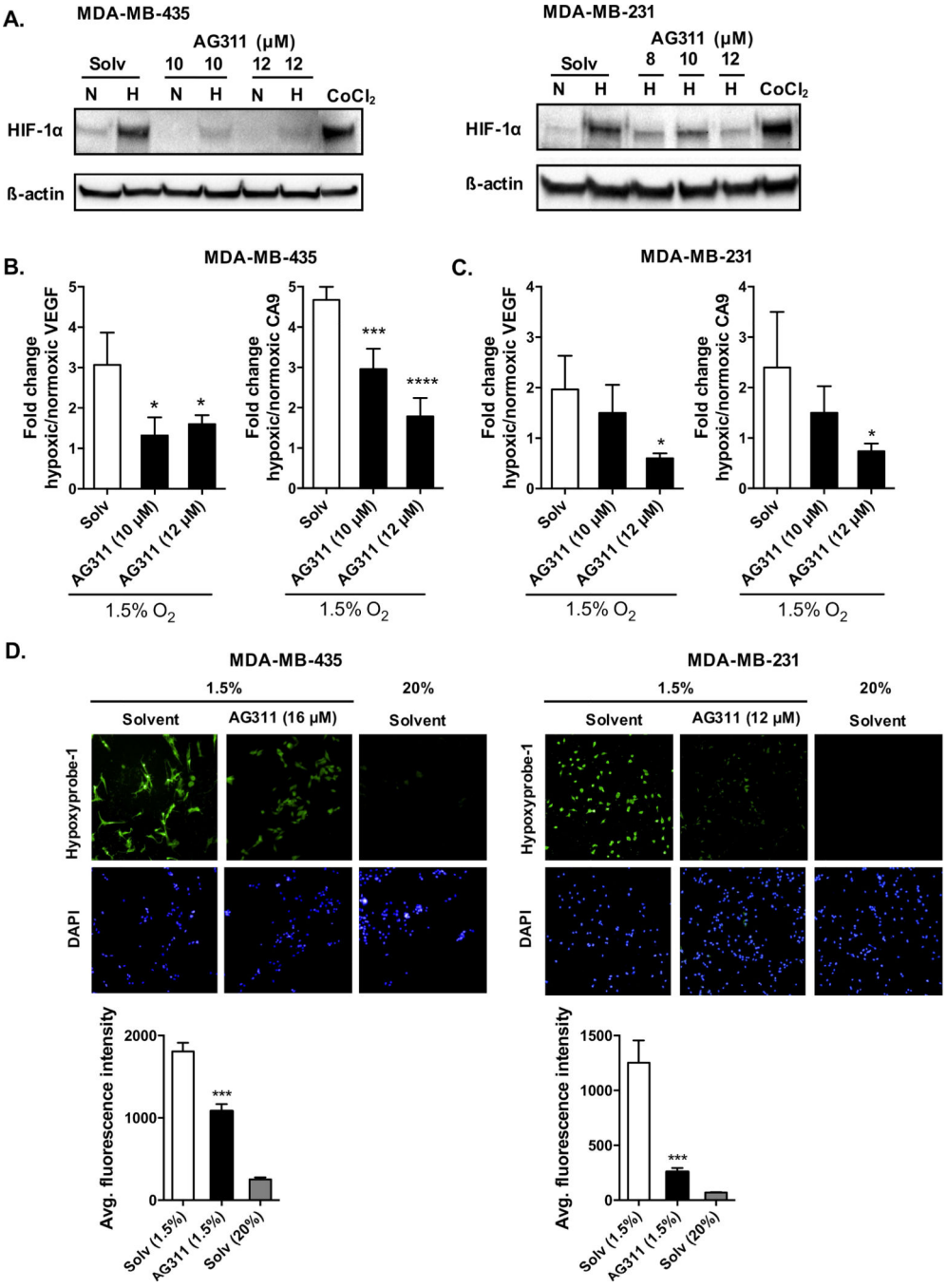

Figure 5. AG311 reduces HIF-1α protein levels, HIF-1α targets genes, and increases oxygen tension in hypoxia

(A). Cells (MDA-MB-435 and MDA-MB-231) were incubated at 20% (N) or 1.5% (H) O_2 for 4 hours in the presence of AG311 followed by protein collection. The hypoxia-mimetic agent $CoCl_2$ (200 μM) was used as a positive control. (n = 4).

(B, C). Real-time PCR analysis of VEGF and CA9 mRNA expression with or without AG311 treatment in hypoxic or normoxic conditions in MDA-MB-435 and MDA-MB-231 cells. Expression was normalized to 28S expression and normoxic controls. (n = 4) **(D)**.

Immunofluorescence images for detection of hypoxia using hypoxyprobe-1. Cells were pretreated with pimonidazole and incubated with or without AG311 for 4 hours in hypoxic or normoxic conditions. DAPI was used to detect nuclei. Quantification of fluorescence intensity in panel below. Data are representative of three independent experiments. (n = 4), $*P \leq 0.01$, $***P \leq 0.001$, $****P \leq 0.0001$ versus solvent control.